Improving Battery Design for Electromagnetic Compatibility: A Magnetic Field Cancellation Method

Yongjun Zhang, *Member, IEEE*, Chenming Zhou, Jacob Carr, and Justin R. Srednicki

***Abstract*—With the increasing demand of power and energy, more and more cells are packed into battery modules. Consequently, the electromagnetic (EM) emissions from batteries also intensify. These emissions have been observed to interfere with nearby electronic safety and health devices, causing malfunctions. While conventional methods, such as shielding, filtering, and distance separation, are commonly used to mitigate the interference issue, each has its own limitations and may not be applicable in all situations. On the other hand, magnetic field cancellation methods found in certain applications offer distinct advantages in addressing challenging magnetic field shielding or compensation issues. In this article, we introduce a novel approach to mitigate EM emissions from batteries consisting of common cylindrical form cells. The new approach leverages the coherent nature of battery cell currents when powering external load and the paired structure present in the battery pack, and then rearranges the cells so that the magnetic fields of the loops of paired cells are canceling one another. We demonstrate the validity of our approach in addressing the EM interference issue that exists in an electronic device currently used in underground coal mines. The results show a significant reduction in EM emission from the battery, highlighting the effectiveness of our approach in real applications.**

***Index Terms*—Battery, cylindrical cell, electromagnetic compatibility, electromagnetic interference (EMI), magnetic field cancellation, multicell battery.**

I. Introduction

TO MEET the ever increasing demand of power and energy, battery manufacturers are responding by packing more cells into their designs. However, this expansion has raised concerns about the electromagnetic (EM) emissions from the battery system and its associated current carrying cable network. For instance, in the electrical vehicles, the high-frequency current ripples created by high-speed switching power converters often constitute a significant source of electromagnetic interference (EMI) [1]. As a result, there has been increasing interest in studying the EM characteristics of batteries in a wide range of frequencies for various purposes and applications [2], [3], [4], [5], [6], [7], [8], [9]. Particular attention has been paid to the cylindrical 18 650 lithium-ion cell due to its cost-effectiveness, energy efficiency, mechanical stability, and widespread use in commercial products [4], [5], [6], [7], [10], [11].

So far, most of the research on battery cell impedance has primarily focused on conductive behavior or emission [3], [4], [5], [6], [7], [12], [13], [14]. Radiated emissions from battery systems have relatively been underexplored. An interesting study delving into the radiated emissions of batteries is found in [15]. In their work, Maleki et al. [15] examined the positions and lengths of the anodic and cathodic tabs within a prism-shaped lithium-ion cell, investigating their impact on the battery's radiated emissions. Their work was further developed into a patent [16], extending to a battery pack composed of multiple prism form cells. In this patent, the asymmetricity of internal electrode construction was harnessed so that the asymmetrical constructions of adjacent cells are oriented in different directions to reduce the overall magnetic field emission. In addition, the internal tab positions are also exploited in the wirings between the cell terminals to achieve further reductions in emission. The primary drawback of this patent is its reliance on prior knowledge of internal asymmetricity and tab positions of battery cell. Consequently, the method described in the patent becomes challenging when dealing with cylindrical 18 650 cells, where it is impractical to know the internal electrode structure and tab positions of each individual battery cell. The method proposed in this article, however, does not rely on the internal battery structure, and hence can be applied to a wide range of battery packs consisting of cylindrical battery cells.

The technique of neutralizing an unwanted magnetic field with a counteracting field, often termed active or dynamic magnetic field cancellation, is a well-established practice in various advanced systems [17], [18], [19], [20]. Naval ships, for instance, employ this method to diminish magnetic signatures and reduce detection risk [21]. The main challenge and drawback of this approach is its complexity and cost, as it requires magnetic sensors, a control system, and EM coils. Nonetheless, this method proves particularly effective in specific scenarios, such as power line applications where the magnetic field's characteristics are predictable, allowing for easier field cancellation. Techniques include modifying power line configurations, splitting and rearranging conductors, mixing phases in super-bundle lines [22], [23], and onboard filtering [24]. To the best of the author's

Manuscript received 15 June 2023; revised 4 October 2023 and 2 April 2024; accepted 16 June 2024. Date of publication 11 July 2024; date of current version 19 February 2025. *(Corresponding author: Yongjun Zhang.)*

The authors are with the National Institute for Occupational Safety and Health (NIOSH), Pittsburgh, PA 15236 USA (e-mail: yzhang13@cdc.gov; czhou@cdc.gov; jcarr1@cdc.gov; jsrednicki@cdc.gov).

Color versions of one or more figures in this article are available at https://doi.org/10.1109/TEMC.2024.3421377.

Digital Object Identifier 10.1109/TEMC.2024.3421377

TABLE I
COMPARISON OF DIFFERENT EMI MITIGATION METHODS ON CYCLONE SIDE OF PDM

	Administrative Control	Shielding	Capacitor filtering	Inductor filtering	New battery design
Method	Increase spacing between devices from 7 to 15.2 cm	Add a copper-mesh pouch on PDM	Add a 4.7 μF capacitor between the two power pins of battery pack	Add 4.7 μH inductor on the positive power pin of battery pack	Redesign battery pack based the method in this article
Performance	9.3 dB reduction at 100 kHz	3.75 dB reduction at 100 kHz	2.0 dB reduction at 100 kHz	13.2 dB reduction at 100 kHz	11 dB reduction at 100 kHz
Disadvantages	Add extra burden on miners; Difficult to maintain all the time	Openings reduce the effectiveness of shielding; Hinders the heat dissipation	Large capacitors are undesirable due to intrinsic safety concerns in mines	Variable voltage drop on power output; Saturation; Intrinsic safety concerns in mines	Add complexity in battery assembly and wiring

knowledge, this technique has not yet been applied to battery systems comprising cylindrical cells. The approach introduced in this article is distinguished by its simplicity and effectiveness, as it does not require additional circuits or external controls, making it highly practical for real-world applications.

Our research on the EM emission of cylindrical battery cells was prompted by the reported incidents of EMI in underground mines [25], [26], [27]. Researchers from the National Institute for Safety and Health (NIOSH) discovered that the EM emission from the battery of the personal dust monitor (PDM) device was the major cause of EMI incidents between the PDM and the wearable proximity detection system (PDS) device [27], [28]. Since then, researchers from NIOSH have been exploring various mitigation strategies [27], [28]. However, none of these methods have been entirely satisfactory. The administrative control method is the simplest and can be achieved by, for example, wearing the two devices on opposite sides of the waist. However, in real environment, it creates extra burden on miners and could be difficult for miners to maintain the separation distance at all times. The shielding pouch did alleviate but could not solve the EMI issue completely. Furthermore, the pouch adds extra weight and size to the device and hinders the dissipation of heat generated by the PDM. The shielding on the battery is constrained by the internal spacing of the PDM. Filtering is another very common and effective EMI mitigation method. However, it requires modification of the circuit board. The cost and time of redesign and recertification process make this approach less attractive. We investigated the structure of the battery and discovered that the cylindrical battery cells in the PDM battery pack are connected in five pairs and placed in parallel. Given the coherence in the currents flowing through each cell, it is therefore possible to rearrange the cells so that the magnetic fields of the five pairs could partially neutralize each other. A practical implementation of this method has demonstrated a significant reduction in EM emissions, especially on the two crucial sides of the PDM battery. We have published a comparative study of this method against others, including administrative control, filtering, and shielding in [29]. A summary of the comparative results is included in Table I. This article presents the detailed steps and analysis of this magnetic field cancellation method on the PDM battery pack and its experimental result.

(a)

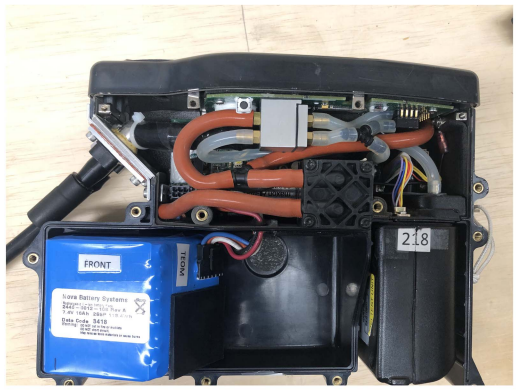

(b)

Fig. 1. Images of PDM devices.

II. PDM BATTERY AND ITS EM EMISSION

Fig. 1 displays the external and internal images of a PDM device that is obligatory for individuals working in underground coal mines. This device continuously monitors the miners' exposure to coal dust, which is crucial to their lung health. If the PDM reports a high dust level, the miners can take necessary precautions, such as improving ventilation or relocating to a different working area. As a result of its critical role in safeguarding miners' health, the Mine Safety and Health Administration mandates the use of PDMs in underground coal mines [30].

The battery of a PDM device is illustrated in Fig. 2, displaying both top and bottom views, as well as an indication of the

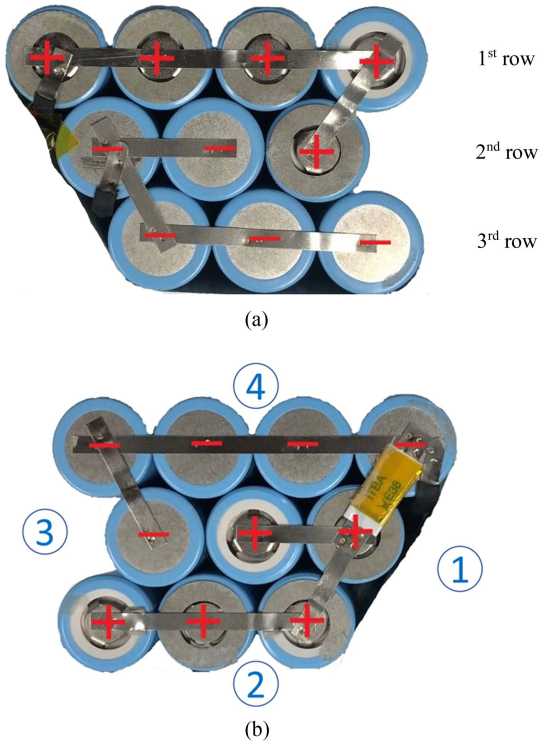

Fig. 2. Top and bottom views of the stock battery: (a) top view and (b) bottom view and the indication of the four sides.

four sides: sides 1– 4 referred in this article. As is shown, the battery comprises ten common cylindrical 18 650-type battery cells, where each cell has a diameter of 18 mm and a height of 65 mm. Every two cells are connected in series, yielding a nominal voltage of 7.4 V. Five pairs of such cells are then connected in parallel to increase the output power, resulting in a so called "5P/2S" configuration.

A. EM Field Simulation

In order to evaluate the EM emission of the battery, we adopt the simplified 3-D structure model for cylindrical 18 650 lithium-ion cell described in [3] and [4], where the battery cell is approximated by a perfect conducting cylinder surrounded by a perfect electrical conductor shield with an opening on the positive side. The inner conducting cylinder has a diameter of 16.73 mm and a length of 64.95 mm, and the outer shield has a diameter of 18.16 mm and a length of 64.95 mm. An external load is placed between the power supply pins of the battery pack, as shown in Fig. 3. The position of each cell model in the battery pack is also shown in Fig. 3. The x-axis is aligned with the edges of the first row of four cells, the y-axis is aligned with the edge of the first cell on the left, and the z-axis extends upward. The bottom plane of battery pack represents the XY-plane at the zero z-axis. The external load and voltage source are adjusted so that each battery cell is supplying a current of 0.5 A.

The EM field simulation is conducted using Altair Feko tool. Fig. 4 displays an image of the magnetic field captured at a distance of 7 cm away from side 1 of the battery. The color

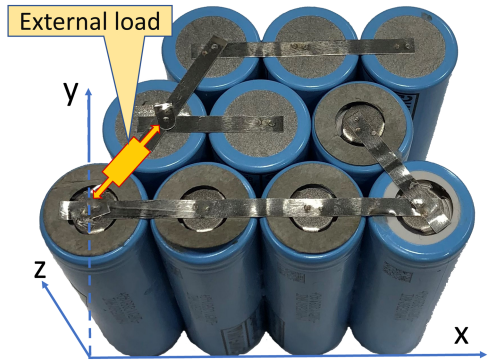

Fig. 3. Positions and orientations of battery cells in XYZ axes and the connection positions of external load in both simulation and experiment.

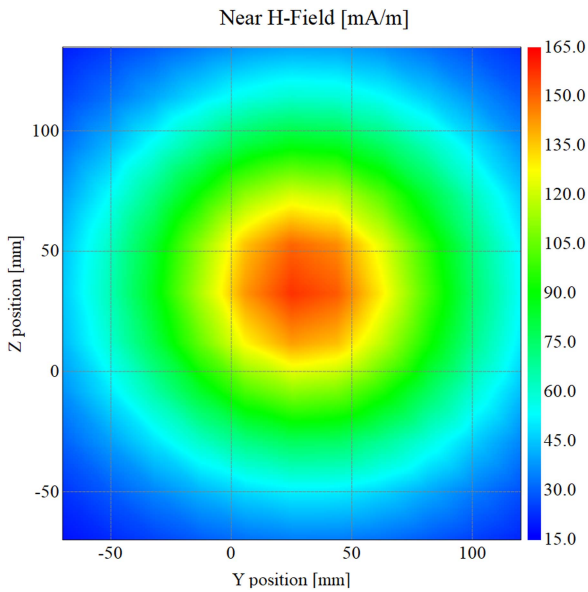

Fig. 4. Simulated magnetic-field plane image at 7 cm away from the edge of side 1 of the stock battery at 100 kHz.

bar illustrates the H-field strength values. As is shown, the maximum magnitude value is around 165 mA/m. Note that the 7-cm distance is adopted from the radiated emission test standard MIL-STD-461 [31]. It is the distance between the antenna and device under test. Side 1 is selected as it corresponds to one of the two sides of the PDM device that exhibits the strong EM emission that could interfere with the operation of nearby PDS devices [26], [27].

According to the simulation, the total radiated power of the stock battery in the far field is about −127.7 dBm at 100 kHz.

B. EM Emission Measurement on Side 1 of the Battery

In addition to simulations, we also performed the EM emission measurement on the real battery using the setup of radiated emission test method (RE101) defined in MIL-STD-461 [31], which serves as de facto standard or the fundamental standard for many industries. As shown in Fig. 12, the battery is placed at a distance of 7 cm from the center of a COM-POWER AL-RE101

passive loop antenna, and the antenna is then connected to a Tektronix RSA5115B spectrum analyzer. To isolate the battery's EM emission from the other components of the external load, i.e., the PDM circuit, a 50-cm-long shielded cable was used to connect the battery to the PDM, and the PDM was then enclosed in a shielded enclosure. The averaged current load of PDM circuit is about 0.5 A.

The spectrum analyzer was configured to measure with 1 kHz resolution bandwidth. To capture the peak EM emission, a thousand sweeps were conducted for approximately 10 s, and then the maximum value of the detected peaks from all the sweeps was recorded using the max-hold function of the spectrum analyzer.

The result of the EM emission measurement on side 1 of the stock battery is displayed as the top red curve in Fig. 13. As shown, there are two primary frequency bands that exhibit strong emissions, one at around 50 kHz, which corresponds to the switching frequency of dc–dc power converters on the board, and the other at around 100 kHz, which corresponds to the driving current frequency of the air pump motor in the PDM. The emission limit specified in MIL-STD-461 standard [31] is also included for reference, which is set at 76 dBpT. Emissions at both bands exceed the limit.

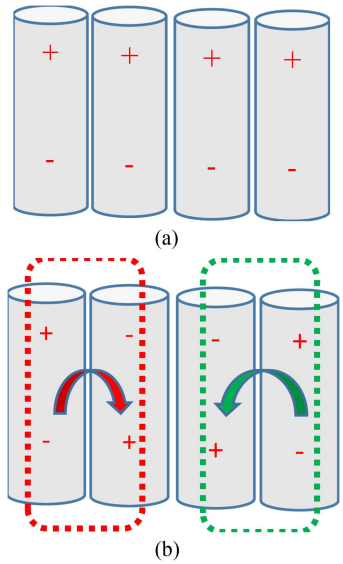

Fig. 5. First row four cells rearrangement of new battery pack. (a) Original four cell arrangement. (b) New four cell arrangement. The red and green arrows indicate the two opposite directions of the current loops of the two paired cells.

III. Novel Approach

During our investigation into the EM emissions from PDM batteries, we discovered that certain multicylindrical-cell batteries can form current loops through pairs or strings of cells. Since they supply power to the same external load, these loops exhibit the same magnitude and phase of current. Inspired by the concept of magnetic field cancellation, we recognized the potential for rearranging the battery cells to exploit these loops. By pairing and overlapping the battery cell loops, we can create opposing current flows. This innovative approach served as the foundation for the design of a new multicylindrical-cell battery pack specifically tailored for PDM devices.

In the following, we delve into the details of this groundbreaking battery pack design, exploring how the arrangement of the battery cells effectively harnesses the principles of magnetic field cancellation to mitigate EM emissions. Let us take another look at the stock battery of the PDM device displayed in Fig. 2. The battery is made up of five pairs of two serially connected battery cells. These pairs of cells form five loops in various ways. It is worth noting that, to keep minimum costs and avoid any modification of the form and structure of existing PDM devices, we want to retain the same structure and shape of the battery pack as that of existing ones.

A. Battery Cell Rearrangement

Now, let us rearrange them in the following manner. In Fig. 5(a), the first row of four cells can be rearranged into two pairs, forming a 2P/2S structure, as shown in Fig. 5(b), so that their current loops have opposite flow directions, as indicated by the red and green arrows in the figure.

The second and third rows of the six cells in Fig. 2(a) can be rearranged, as shown in Fig. 6, forming a 3P/2S structure. The pair of middle cells is arranged such that it has current flow in the opposite direction to those of the two adjacent pairs.

B. Simplified Analysis on Magnetic Field Cancellation

The radiated EM emission of a battery cell is closely linked to the inductive impedance of the battery cell. According to [7] and [32], the inductive impedance of cylindrical cell is composed by three parts: the cell's coiled structure, the interaction between the anode and cathode current collectors, and the length of the cell along which current travels longitudinally from the anode to the cathode terminal. Due the complicated electrochemical processes, as well as its physical spiral structure, the inductance of battery cell is rather complicated and decreases nonlinearly when frequency increases [32].

For the simplicity of our analysis, in the following, we assume battery as a solid cylindrical conductor with length l and radius r. We also assume that the effect of the end connections between the conductors can be ignored and the current is uniformly distributed over the cross section of the conductor.

The self-inductance of such a cylindrical conductor can be calculated as follows [33], [34], [35]:

$$L_{\text{self}} \approx \frac{\mu_0 l}{2\pi}\left(\ln\frac{2l}{r} - \frac{3}{4}\right) \tag{1}$$

where μ_0 is the permeability of the air.

When two conductors are placed nearby in parallel, the time-varying magnetic field created from one conductor will impact the EM field behavior of the other one. Let us consider the parallel case in Fig. 7(a), where two conductors carry currents in the same direction. According to [33], [34], and [35], their total inductance can be calculated by the summation of self-inductance and mutual inductance from the other

$$L_{\text{parallel}} = 2\left(L_{\text{self}} + M_d\right). \tag{2}$$

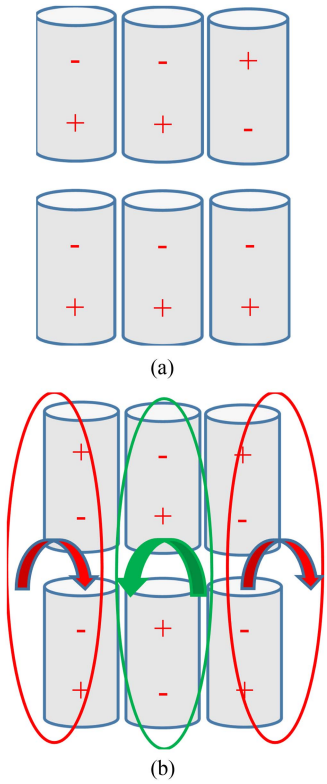

Fig. 6. Second and third rows of battery cell rearrangement. (a) Original six cell arrangement. (b) New six cell arrangement. The red and green arrows indicate the different directions of the current loops of the three paired cells.

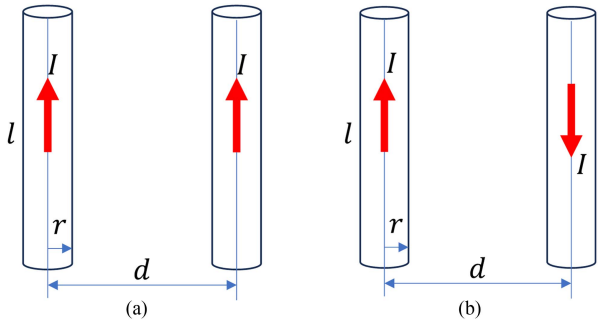

Fig. 7. Inductance of two straight conductors. (a) Two parallel conductors where current flow in the same directions. (b) Two anti-parallel conductors where current flow in opposite directions.

Here, M_d denotes the mutual inductance between the two conductors with a separation distance d between the centers. The mutual inductance M_d can be approximated by the following [33], [34], [35]:

$$M_d \approx \frac{\mu_0 l}{2\pi}\left(\ln\frac{2l}{d} - 1 + \frac{d}{l}\right). \tag{3}$$

Note, the above formula assumes that the length l is much greater than the separation distance d. A shorter relative length would need a more complicated formula.

In the case where two conductors carry currents in opposite directions, as shown the antiparallel case in Fig. 7(b), their inductance is given by the following [33], [34], [35]:

$$L_{\text{antiparallel}} = 2\left(L_{\text{self}} - M_d\right). \tag{4}$$

These calculations, often referred to as the Grover method [34], can be applied to an array of multiple conductors [33], [34]. Assuming that the four battery cells in Fig. 5 can be simplified as four cylindrical conductors, we can estimate the total inductance for the arrangement in Fig. 5(a) as follows:

$$L_{\text{org4}} = 4L_{\text{self}} + 6M_d + 4M_{2d} + 2M_{3d} \tag{5}$$

and for the new arrangement in Fig. 5(b) as follows:

$$L_{\text{new4}} = 4L_{\text{self}} - 2M_d - 4M_{2d} + 2M_{3d}. \tag{6}$$

Substituting l with 65 mm, r with 9 mm, and d with 19 mm in above formulas, we arrive at approximate inductances of 255 nH for the original arrangement L_{org4} and 44 nH for the new one L_{new4}.

The above analysis is overly simplified and the approximations may be far from accurate. However, the underlying concept still holds. Altering the direction of current flow among the conductors can decrease the total inductance, especially when compared to an arrangement where currents in all conductors are flowing in the same direction. The difference in inductance depends on the mutual inductance; the larger the mutual inductance, the greater the difference.

It is noteworthy that, through the 3-D EM simulation and experiment, Landinger et al. [32] demonstrated that the Grover method is also applicable to two parallel cylindrical battery cells. In other words, the principle also applies to the battery cells in Figs. 5 and 6, such that the new arrangement has less inductance than the original arrangement. The extent of reduction largely depends on the mutual coupling of the battery cells. The inductive mutual coupling of two cylindrical 18 650 battery cells, connected in series and placed in parallel, has been well studied in [32]. It was found that the mutual inductance is relatively small below 1 MHz but increases significantly between 1 and 20 MHz.

C. Battery Pack Wiring

With the position of each cell being fixed, the subsequent step involves choosing a wiring option. Note that the wiring on the bottom is fixed due to the pairing. There are several wiring options for connecting the cathodes and anodes of cells located on the top of the battery pack. Each top wiring option results in a unique current flow pattern, depending on the placement of the external load. For example, Fig. 8 shows one wiring option where all the anodes on the top are connected to single place with straight wires, and so are all the cathodes. However, this wiring configuration poses a safety concern and/or manufacture challenge as some positive and negative wires overlap, potentially resulting in electrical shorts if insulation materials wear out or are not properly placed.

An alternative and better top wiring option, which eliminates wire crossover, is illustrated in Fig. 9(a) and (b). We adopted this option, and the actual PDM battery pack based on this wiring option is shown in Fig. 9(c) and (d).

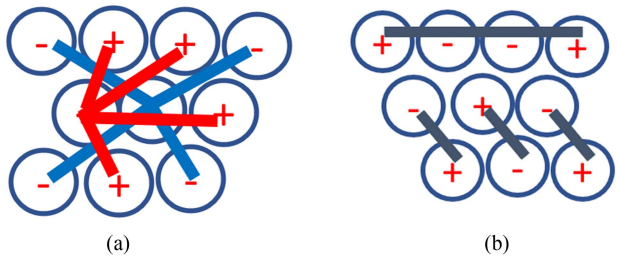

Fig. 8. Wiring diagram option #1 with wire crossovers. (a) Top wiring diagram. (b) Bottom wiring diagram.

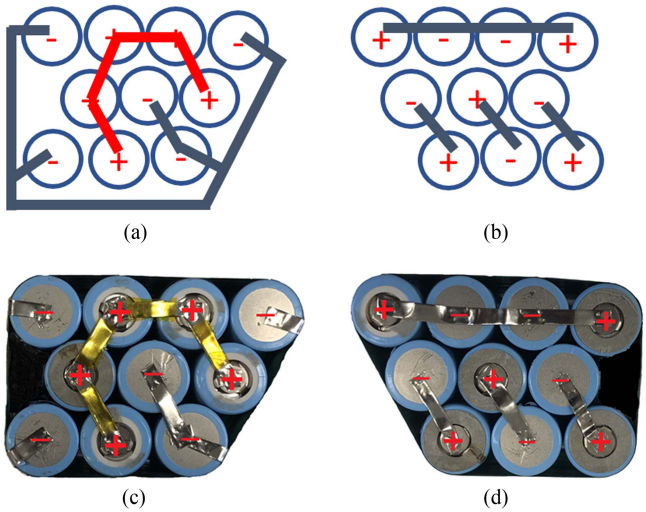

Fig. 9. Wiring diagram option #2 without wire crossover. (a) Top wiring diagram. (b) Bottom wiring diagram. (c) Top view of the real battery. (d) Bottom view of the real battery.

IV. Result of New PDM Battery Design

As in Section II, we assess the EM emission of the new battery design using both simulation and experimental measurement. Then, we will compare the results with that of the stock battery.

A. EM Field Simulation

The EM simulation of the new battery was conducted using the same simplified 3-D structure for the battery cell as described in Section II-A. The external load was placed on the two power supply pins depicted in Fig. 10. The XYZ axes are the same as that in Fig. 3.

Fig. 11 displays the magnetic field plane image captured at 7 cm away from side 1 of the new battery. In comparison to Fig. 3, the maximum near-field strength value on side 1, as indicated by the color bar, has decreased from 165 to 22 mA/m. It is important to note that this comparison only considers the maximum field magnitude value and does not take into account the phase and direction of the magnetic field, which are also crucial factors in measuring actual EM emissions.

Based on the simulation result, the total radiated power of the new battery in the far field is about −132.2 dBm at 100 kHz, about 4.5 dB reduction compared with that of the stock battery.

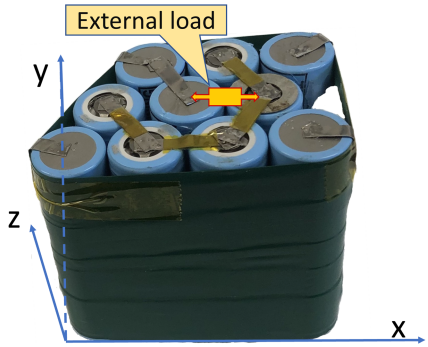

Fig. 10. Top view of positions, orientations, and wirings of battery cells, and the connection positions of external load in both simulation and experiment.

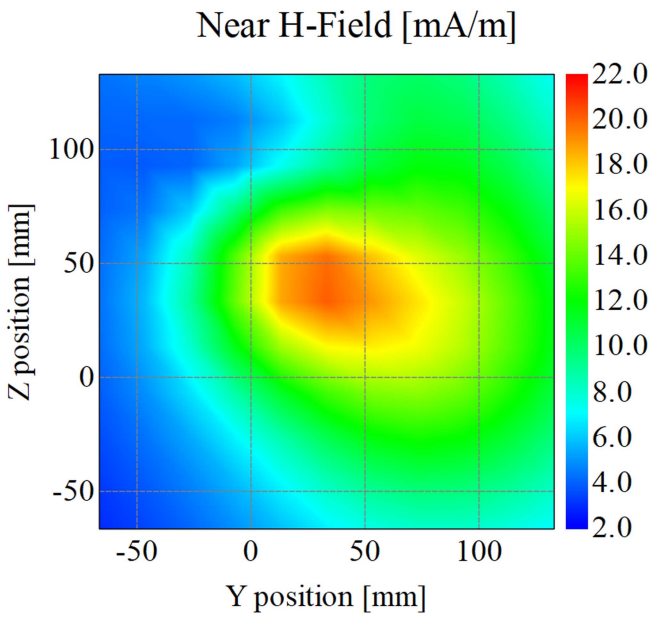

Fig. 11. Simulated magnetic-field plane image at 7 cm away from the edge of side 1 of the new battery at 100 kHz.

B. EM Emission Measurement on Side 1 of the Battery

We used the same measurement setup shown in Fig. 12 to measure the EM emission of the new battery, as we did for the stock battery. The result from side 1 of the new battery is presented as the blue curve in Fig. 13, indicating a remarkable reduction in EM emissions compared with those of the original stock battery, with an approximately 18 dB decrease at 100 kHz.

C. EM Emission Reductions on Other Sides of Battery

Because the magnetic field cancellation appears almost on every side of the battery pack, we expect that the decrease in EM emissions is not limited to one side of the new battery. Indeed, it is present in a similar measure on other sides as well. This observation is supported by experimental measurements. Fig. 14 illustrates the reduction in measured EM emissions on other sides of the battery.

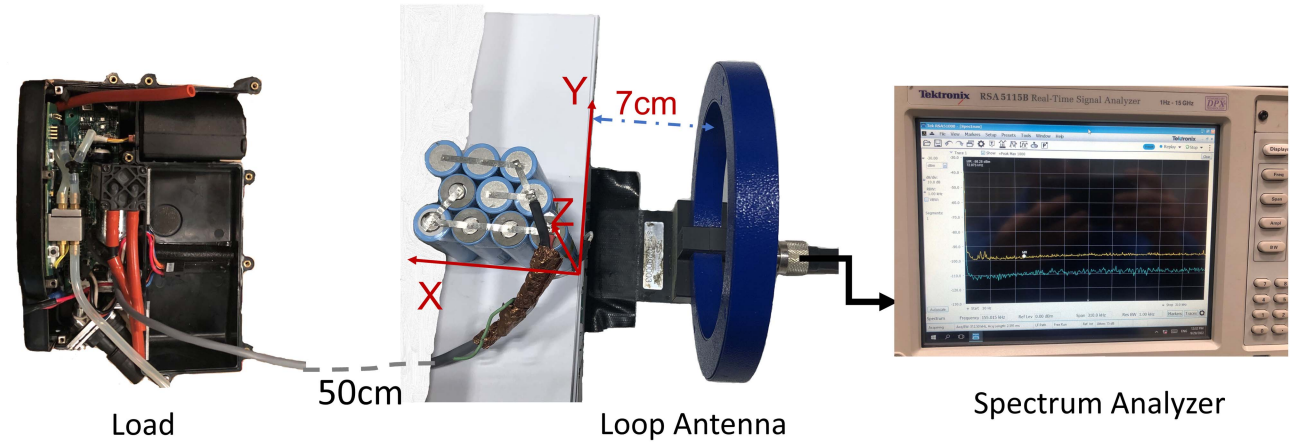

Fig. 12. Battery EM emission measurement setup.

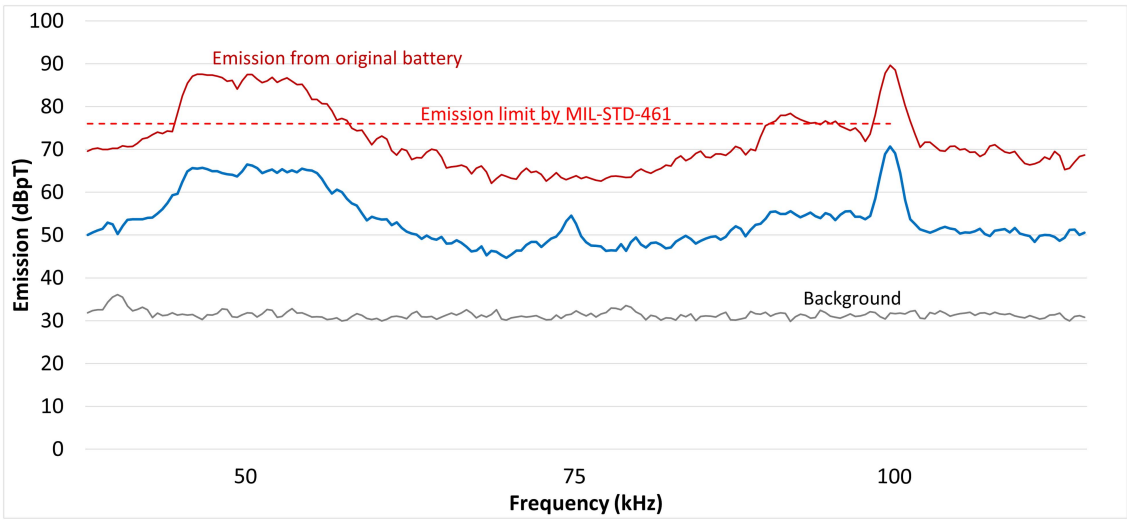

Fig. 13. Measured EM emission comparison of side 1 of new battery versus that of original stock battery.

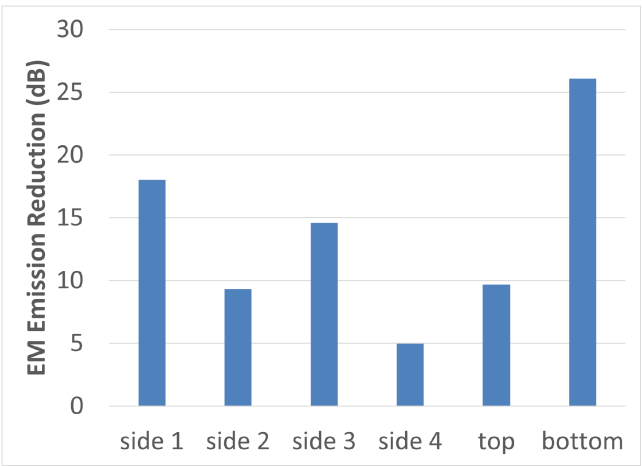

Fig. 14. Measured EM emission reduction of all sides of the new battery, compared with the stock battery.

D. Comparison With Other EMI Mitigation Methods in a PDM Device

As mentioned in Section I, this newly designed battery pack was applied to a PDM device, and its EMI mitigation performance was compared with conventional methods, such as administrative control, filtering, and shielding. The results were published in [29]. For reference, a summary of the comparative results is presented in Table I.

V. Conclusion

The fact that batteries can be a source of radiated EM emission has not been well conceived by many engineers. This issue is exemplified by the EMI problem between the PDM and the PDS devices, which demonstrates that the EM emission from batteries can be severe and catch us off guard. While conventional methods, such as shielding and filtering, do help mitigate EMI, they can be costly and come with tradeoff, especially when the product is on the market.

However, through simulation and experimental measurement, we have found that magnetic field cancellation techniques can effectively reduce EM emissions from multicell battery packs. By rearranging the positions of battery cells, we were able to achieve a significant reduction in EM emissions. Our initial result was first presented as a one-page abstract [36] in conference. One of the key advantages of our approach is that it effectively addresses the EMI issue between the PDM and the PDS without requiring any modifications to the existing PDM circuit boards. This is significant as it saves both time and money, because any redesign and recertification of coal mining devices is time consuming and costly.

There are a few interesting topics that merit further investigation. For instance, what are the best battery pack designs that have least possible EM emissions? How can this method be applied to large numbers of battery cells? What are the best wiring practices for minimal EM emission for large battery pack?

It should be noted that the new arrangement of the PDM battery cells might introduce added complexity in the jointing of anodes and cathodes. Despite this, we believe that our approach provides valuable new insights and potential solutions for battery designers and manufacturers looking to improve EM compatibility in their products.

In this work, the battery cell is approximated as a simple 3-D structure. While this simplified model served our initial needs for comparing the simulated results of the stock and new battery, we believe that there is still ample room for further exploration on the radiated emission of the battery cells and packs. For example, our next step is to investigate and correlate simulated radiated emissions with measured radiated emissions. Another interesting venue of the study is investigating the impact of the defects, such as short-circuit or aging of battery cells, on the EM field. Quantifying the effects of unbalanced cells resulting from these defects would provide valuable insights. These research topics will contribute to enhancing our understanding of EM field characteristics in the battery systems and could lead us to find new methods in detecting and maintaining the health of the battery.

ACKNOWLEDGMENT

The findings and conclusions in this article are those of the authors and do not necessarily represent the official position of the National Institute for Occupational Safety and Health (NIOSH), Centers for Disease Control and Prevention (CDC). Mention of any company name or product does not constitute endorsement by NIOSH.

REFERENCES

[1] H. Li et al., "Lithium-ion battery modeling under high-frequency ripple current for co-simulation of high-power DC-DC converters," *J. Energy Storage*, vol. 54, 2022, Art. no. 105284.

[2] E. Hoene, S. Guttowski, R. Saikly, W. John, and H. Reichl, "RF-properties of automotive traction batteries," in *Proc. IEEE Int. Symp. Electromagn. Compat.*, 2003, pp. 425–428.

[3] A. R. Ruddle, Y. X. Teo, and J. Chen, "Electromagnetic modelling strategies for EMC analysis of automotive traction batteries," in *Proc. Int. Conf. Electromagn. Adv. Appl.*, 2017, pp. 1395–1398.

[4] A. R. Ruddle, J. Chen, and Y. X. Teo, "Measurement of RF impedance for automotive 18650 cylindrical lithium ion cells," in *Proc. Int. Symp. Electromagn. Compat.*, 2017, pp. 1–6.

[5] P. K. P. Ferraz, R. Schmidt, D. Kober, and J. Kowal, "A high frequency model for predicting the behavior of lithium-ion batteries connected to fast switching power electronics," *J. Energy Storage*, vol. 18, pp. 40–49, 2018.

[6] T. F. Landinger, G. Schwarzberger, and A. Jossen, "A physical-based high-frequency model of cylindrical lithium-ion batteries for time domain simulation," *IEEE Trans. Electromagn. Compat.*, vol. 62, no. 4, pp. 1524–1533, Aug. 2020.

[7] T. F. Landinger, G. Schwarzberger, and A. Jossen, "High frequency impedance characteristics of cylindrical lithium-ion cells: Physical-based modeling of cell state and cell design dependencies," *J. Power Sources*, vol. 488, 2021, Art. no. 229463.

[8] T. F. Landinger et al., "Power line communications in automotive traction batteries: A proof of concept," in *Proc. IEEE Int. Symp. Power Line Commun. Appl.*, 2020, pp. 1–5.

[9] I. Ouannes, P. Nickel, and K. Dostert, "Cell-wise monitoring of Lithium-ion batteries for automotive traction applications by using power line communication: Battery modeling and channel characterization," in *Proc. 18th IEEE Int. Symp. Power Line Commun. Appl.*, 2014, pp. 24–29.

[10] C. Jiaqi, A. R. Ruddle, and Y. X. Teo, "Predicting the RF impedance of cells in series for automotive traction battery applications," in *Proc. Int. Symp. Electromagn. Compat.*, 2017, pp. 1–6.

[11] H. Hackl, D. J. Pommerenke, M. Ibel, and B. Auinger, "Extraction of single cell impedance from battery module measurement by simulation-based de-embedding," *IEEE Trans. Signal Power Integrity*, vol. 1, pp. 112–120, 2022.

[12] F. C. Laman, M. W. Matsen, and J. A. R. Stiles, "Inductive impedance of a spirally wound Li/MoS2 cell," *J. Electrochem. Soc.*, vol. 133, no. 12, 1986, Art. no. 2441.

[13] M. Guo and R. E. White, "Mathematical model for a spirally-wound lithium-ion cell," *J. Power Sources*, vol. 250, pp. 220–235, 2014.

[14] S. Schindler and M. A. Danzer, "Influence of cell design on impedance characteristics of cylindrical lithium-ion cells: A model-based assessment from electrode to cell level," *J. Energy Storage*, vol. 12, pp. 157–166, 2017.

[15] H. Maleki, R. Zurek, J. N. Howard, and J. A. Hallmark, "Lithium ion cell/batteries electromagnetic field reduction in phones for hearing aid compliance," *Batteries*, vol. 2, no. 2, 2016, Art. no. 19.

[16] H. Maleki and J. A. Hallmark, "Electrochemical battery pack with reduced magnetic field emission and corresponding devices," U.S. Patent US8642205B2, 2014.

[17] H. E. Peters, H. B. Owings, and P. A. Koppang, "Atomic hydrogen masers with self auto—Tune system and magnetic field cancellation servo," in *Proc. 20th Ann. Precise Time Interval Syst. Appl. Meeting*, 1988, pp. 337–344.

[18] M. H. Acuna et al., "Magnetic field cancellation techniques for the Mars Global Surveyor solar array," in *Proc. IEEE Photovolt. Specialists Conf.*, 1996, pp. 325–328.

[19] O. Baltag, D. Costandache, M. Rau, A. Iftemie, and I. Rau, "Dynamic shielding of the magnetic fields," *Adv. Elect. Comput. Eng.*, vol. 10, no. 4, pp. 135–142, 2010.

[20] D. Platzek, H. Nowak, F. Giessler, J. Röther, and M. Eiselt, "Active shielding to reduce low frequency disturbances in direct current near biomagnetic measurements," *Rev. Sci. Instruments*, vol. 70, no. 5, pp. 2465–2470, 1999.

[21] J. J. Holmes, "Reduction of a ship's magnetic field signatures," *Synth. Lectures Comput. Electromagn.*, vol. 3, no. 1, pp. 1–68, 2008.

[22] J. C. Bravo-Rodríguez, J. C. del-Pino-López, and P. Cruz-Romero, "A survey on optimization techniques applied to magnetic field mitigation in power systems," *Energies*, vol. 12, no. 7, 2019, Art. no. 1332.

[23] O. Bottauscio et al., "CIGRE guidelines for mitigation techniques of power-frequency magnetic fields originated from electric power systems," 2009.

[24] M. F. da Silva, L. M. Honório, A. L. M. Marcato, V. F. Vidal, and M. F. Santos, "Unmanned aerial vehicle for transmission line inspection using an extended Kalman filter with colored electromagnetic interference," *Instrum. Soc. Amer. Trans.*, vol. 100, pp. 322–333, 2020.

[25] J. Noll et al., "Electromagnetic interference with proximity detection systems," in *Proc. Annu. Conf. Soc. Mining, Metall. Exploration*, no. 17-053, 2017.

[26] J. Noll et al., "Electromagnetic interference from personal dust monitors and other electronic devices with proximity detection systems," *Mining Eng.*, vol. 70, no. 5, 2018, Art. no. 61.

[27] J. Li, J. Carr, M. Reyes, C. Jobes, B. Whisner, and P. McElhinney, "Mitigation of RF radiation and electromagnetic interference from a lithium-ion battery pack used in wearable safety and health devices in the mining industry," in *Proc. Photon. Electromagn. Res. Symp.-Spring*, 2019, pp. 3601–3608.

[28] J. Noll, C. DeGennaro, J. Li, C. Zhou, and J. Srednicki, "Evaluation of different shielding materials for reducing electromagnetic interference of the personal dust monitor 3700," in *Proc. SME Annu. Meeting Exhibit*, no. 18-078, 2018.
[29] Y. Zhang et al., "A comparison of EM emission reduction methods for personal dust monitors," in *Proc. SME Annu. Meeting*, no. 23-005, 2023.
[30] "Mandatory health standards - underground coal mines subpart C - Sampling procedures § 70.201 sampling; general and technical requirements." Accessed: Feb. 15, 2022. [Online]. Available: https://www.ecfr.gov/current/title-30/chapter-I/subchapter-O/part-70
[31] *Requirements For The Control Of Electromagnetic Interference Characteristics Of Subsystems And Equipment*, MIL-STD-461 EMC Standard. Accessed: Dec. 1, 2022. [Online]. Available: https://quicksearch.dla.mil/qsDocDetails.aspx?ident_number=35789
[32] T. F. Landinger, G. Schwarzberger, G. Hofer, M. Rose, and A. Jossen, "Power line communications for automotive high voltage battery systems: Channel modeling and coexistence study with battery monitoring," *Energies*, vol. 14, no. 7, 2021, Art. no. 1851.
[33] E. B. Rosa and F. W. Grover, *Formulas and Tables for the Calculation of Mutual and Self-Inductance*. Washington, DC, USA: National Bureau of Standards, 1912.
[34] F. W. Grover, *Inductance Calculations: Working Formulas and Tables*. Mineola, N.Y., USA: Dover Publications, 2004.
[35] E. B. Rosa, *The Self and Mutual Inductance of Linear Conductors*. Washington, DC, USA: National Bureau of Standards, 1908.
[36] Y. Zhang, C. Zhou, and J. Srednicki, "EMI control for a multi-cell battery," in *Proc. IEEE Int. Symp. Electromagn. Compat., Signal Power Integrity*, 2022, pp. 596–596.

Yongjun Zhang (Member, IEEE) received the Ph.D. degree in electrical and computer engineering from the University of Delaware, Newark, Delaware, in 2001.

Before his career with Yinzcam, he was a Research Scientist with Intrigue Technology Inc., and then an embedded Systems Engineer with 360 Fly Inc. Earlier, he was an ASIC Engineer with Oki Semiconductor, in Pittsburgh, PA, USA. In 2021, prior to joining the National Institute for Occupational Safety and Health (NIOSH), he was a Senior Software Engineer with Yinzcam Inc. He is currently the Project Leader and Principal Investigator for the project of EMI and EMC considerations in underground mines with the NIOSH, part of the Centers for Disease Control and Prevention, under the U.S. Department of Health and Human Services.

Chenming Zhou received the Ph.D. degree in electrical engineering from Tennessee Technological University, Cookeville, TN, USA, in 2008.

He was the Project Leader and Principal Investigator for the wireless communications and tracking project, and later the Internet of Things for underground coal mines project with the National Institute for Occupational Safety and Health (NIOSH). Prior to his industry career with Disney, he was a Project Research Scientist with the Department of Electrical and Computer Engineering, Carnegie Mellon University, Pittsburgh, PA, USA. He currently holds the position of Team Lead with the NIOSH, part of the Centers for Disease Control and Prevention, under the U.S. Department of Health and Human Services. He is also a Government Contract Officer Representative for NIOSH overseeing Broad Agency Announcement contracts that concentrate in communications, tracking, sensing, and data analytics. He holds two U.S. patents in RFID and is the author or coauthor of more than 80 technical papers published in journals or conference proceedings.

Dr. Zhou was an Associate Editor for *IEEE Antennas and Propagation Magazine* from 2015 to 2021, and is currently an Associate Editor for the *Mining, Metallurgy & Exploration Journal*. Prior to joining NIOSH in 2012, he was a Research Fellow with the Disney Research Laboratory, Pittsburgh, where he conducted research in RF ranging based on passive RFID tags.

Jacob Carr received the B.S. and M.S. degrees in mining engineering from the University of Nevada, Reno, NV, USA, in 2006 and 2008, respectively, and the Ph.D. degree in energy and mineral engineering from Penn State, University Park, PA, USA, in 2019.

He is the Deputy Branch Chief for the Health Hazards Prevention Branch within the Pittsburgh Mining Research Division of NIOSH. He is also the Coordinator for the NIOSH Center for Occupational Robotics Research (CORR). Prior to taking this position, he was the Team Leader for NIOSH's Mining Technologies Team, where his research interests include proximity detection, collision avoidance, electromagnetic interference, and other topics.

Justin R. Srednicki received the A.S. degree in electrical engineering technology from Pittsburgh Technical Institute, Oakdale, PA, USA, in 2007.

Since 2007, he has been an Electronic Technician with the National Institute for Occupational Safety and Health (NIOSH)/Pittsburgh Mining Research Division, Pittsburgh, PA. He began his career with NIOSH in 2007. His research focuses on promoting mine safety research through his involvement with emergency communication and tracking systems, mine illumination, intrinsic battery safety, refuge alternatives, proximity detection and collision avoidance systems, and electromagnetic interference.